Title
Measurements of radiation characteristics of fused quartz containing bubbles.

Journal
Journal of the Optical Society of America. A, Optics, image science, and vision, 21(1)

ISSN
1084-7529

Authors
Baillis, Dominique
Pilon, Laurent
Randrianalisoa, Harifidy
et al.

Publication Date
2004

Peer reviewed

Measurements of Radiation Characteristics of Fused Quartz Containing Bubbles

Dominique Baillis

Centre de Thermique de Lyon, INSA Lyon, 69621 Villeurbanne, France

Laurent Pilon

Mechanical and Aerospace Engineering Department

University of California, Los Angeles, CA 90095, USA

E-mail: pilon@seas.ucla.edu

Harifidy Randrianalisoa

Centre de Thermique de Lyon, INSA Lyon, 69621 Villeurbanne, France

Rafael Gomez

School of Electrical and Computer Engineering

Purdue University - West Lafayette, IN 47907, USA

Raymond Viskanta

School of Mechanical Engineering

Purdue University - West Lafayette, IN 47907, USA

This paper reports experimental measurement of radiation characteristics of fused quartz containing bubbles over the spectral region from 1.67 to 3.5 μm. The radiation characteristics were retrieved by an inverse method that minimizes the quadratic difference between the measured and calculated spectral bi-directional transmittance and reflectance for different sample thicknesses. The theoretical spectral transmittances and reflectances were computed by solving the one-dimensional radiative transfer equation by the discrete ordinates method for a non-emitting, homogeneous, and scattering medium. The results of the inversion were shown to be independent of the sample thickness for samples thicker than 3 mm and clearly demonstrate that bubbles have an effect on the radiation characteristics of fused quartz.

OCIS codes: 000.0000, 999.9999.

1. INTRODUCTION

The radiative transfer equation (RTE) describes on a phenomenological level radiation transfer in a continuous, homogeneous medium while porous media consist of a dispersed and a continuous phase and, therefore, are by nature inhomogeneous [1]. However, the theory can still be employed using the effective absorption and scattering coefficients and the effective phase function of the porous medium provided that the porous medium can be treated as homogeneous, i.e., if the pore size to sample dimension ratio is very small. However, no quantitative model is currently available to predict the minimum material thickness beyond which the homogeneous assumption

is valid. Numerous studies have been performed on theoretical predictions and experimental determination of thermal radiation characteristics of heterogeneous media. A review on the subject has been recently presented by Baillis and Sacadura [2].

The literature contains numerous studies concerned with closed-cell foams such as polyurethane or polystyrene foams [3–7]. All of them consider the medium to be optically thick and isotropically scattering materials for which the Rosseland diffusion approximation is valid. This approach consists of treating the radiative transfer as a diffusion process. Then, one may define a radiative conductivity k_R by [1]

$$k_R = \frac{16 n^2 T^3}{3\beta_R} \tag{1}$$

where σ is the Stefan-Boltzmann constant ($= 5.670 \times 10^{-8}$ W/m^{2}K^4) and n is the effective index of refraction of the heterogeneous medium. The dependence of the latter on wavelength is negligible compared with that of the extinction coefficient β_λ and its value is close to unity for large porosity [8].The Rosseland-mean extinction coefficient β_R can be computed from its definition,

$$\frac{n^2}{\beta_R} = \frac{\pi}{4\sigma T^3} \int_0^\infty \frac{(n_\lambda^c)^2}{\beta_\lambda} \frac{\mathrm{d}I_{b,\lambda}}{\mathrm{d}T} \mathrm{d}\lambda \tag{2}$$

where $\frac{\mathrm{d}I_{b\lambda}}{\mathrm{d}T}$ is the derivative of the blackbody spectral intensity $I_{b,\lambda}$ with respect to temperature T.

When the porous medium cannot be treated as optically thick or isotropically scattering more refined models for radiation characteristics are required. For example, fused quartz or soda-lime silicate glasses are weakly absorbing in the spectral range from 0.2 μm to approximately 4.5μm [9, 10] and the Rosseland diffusion approximation may not be valid. Pilon and Viskanta [11] discussed extensively the model for

radiation characteristics of semitransparent media containing bubbles proposed by Fedorov and Viskanta [12, 13] and applied it to soda-lime silicate glass containing bubbles having radius larger than 10 μm and porosity between 0 and 0.74. The results for soda-lime silicate glass indicate that scattering of radiation by the bubbles entraped in the glass matrix dominates the radiation transfer for porosity larger than 0.2 in the spectral range from 0.3 to 4.5 μm where the glass is weakly absorbing. For longer wavelengths, however, the glass matrix is strongly absorbing and absorption by the matrix dominates the radiation transfer [11].

The present study is restriced to radiation characteristics of semitransparent media containing bubbles. Experimental evidence on the effect of voids on the radiation characteristics of fused quartz containing bubbles is presented. First, different techniques for measuring the radiation characteristics of porous materials reported in the literature are briefly reviewed. Then, the experimental setup and procedure to retrieve the radiation characteristics by an inverse method are presented. Finally, experimental results are discussed along with a parametric study of the experimental conditions and assumptions made to retrieve the radiation characteristics.

2. Current State of Knowledge

Established techniques for estimating the radiation characteristics of porous materials consist of measuring some apparent physical quantities of the medium and of using inverse methods to retrieve the radiation characteristics that best fit the experimental data by solving the RTE. Initial values for the radiation characteristics are assumed and the RTE is solved. Then, the calculated and measured apparent properties are

compared and a new estimate is made. This procedure is accomplished in an iterative manner until the set of absorption and scattering coefficients and phase function minimizes the difference between the measured and the calculated apparent properties. The major drawbacks inherent to the inverse method is that the problem is ill-posed, i.e., there is no unique solution for the absorption and scattering coefficients and the scattering phase function. Moreover, due to the iterative nature of the method, the initial value for the absorption and scattering coefficients are of major importance if one wants a rapid convergence of the solution. Experimental measurements commonly associated with inverse methods to retrieve the radiation characteristics of porous media are (i) spectral or total, (ii) directional-hemispherical or directional-directional measurements of transmittance and reflectance, and (iii) collimated (normal or not) or diffuse incident radiation. Moreover, several numerical techniques have been used to solve the RTE along with different optimization algorithms to minimize the difference between predictions and experimental data.

Hale and Bohn [14] combined the Monte-Carlo method with importance sampling and a nonlinear least squares convergence technique to compute the absorption and scattering coefficients of reticulated alumina foams from the spectral directional-hemispherical transmittance assuming an isotropic phase function. The directional-hemispherical transmittances of three samples of different thicknesses were measured. The initial guess for the radiation characteristics were obtained from a simplified geometric model.

Hendricks and Howell [15] derived the radiation characteristics of reticulated porous ceramics by measuring their spectral directional-hemispherical transmittance

and reflectance for $0.4\mu\text{m} < \lambda < 5\mu\text{m}$. They used the traditional inverse method with the discrete ordinates method to solve the RTE and a nonlinear-least squares minimization algorithm. They investigated two different phase functions with two unknown parameters. The samples were 1-2 mm thick with 10 to 65 pores per inch (ppi) and a porosity of 80-85%. The authors reported severe computational stability and accuracy requirements and obtained only a few successfully converged optimum solutions, particular for most scattering samples (65 ppi). Moreover, the samples were thin to enable transmittance measurement but the homogeneity assumption may not be valid as reported by Hale and Bohn [14] for similar methods.

Baillis *et al.* [16] have determined radiation characteristics of open-cell carbon foams by using a prediction model based on geometric optics combined with diffraction. Baillis and co-workers [17, 18] combined measurements of bi-directional and directional-hemispherical transmittance and reflectance to identify the radiative characteristics of polyurethane foams. They solved the RTE by the discrete ordinates method. Their study shows that a combination of bi-directional and directional-hemispherical measurements provides complementary information and is preferable over either bi-directional or directional-hemispherical measurements. As mentioned by Baillis *et al.* [17], the drawbacks of using bi-directional measurements for highly forward scattering media is the weakness of the transmitted or reflected signal in directions other than the normal direction that leads to high experimental uncertainties. On the other hand, only directional-hemispherical measurements for a given sample thickness do not permit the estimation of the scattering phase function that often is assumed to be isotropic [18]. Moura [19] recovered the spectral radiation

characteristics of different fibrous media from spectral transmittance and reflectance measurements with different angles of incidence. However, the authors assumed that the scattering phase function was azimuthally symmetric which limits the generality of the approach.

All the above mentioned studies have assumed that the porous medium can be treated as homogeneous. Such an assumption leads to the following experimental dilemma: on the one hand, one needs thick enough samples to be able to apply the inverse method using the RTE, yet, on the other hand some porous media are so highly scattering and/or absorbing that the signal of the transmitted radiation is very weak even for thin samples, and the experimental uncertainty is very large. Moreover, if a thick layer is exposed to a high intensity of radiation to obtain stronger signals, the incident radiation may heat up the sample causing non-uniformity in the sample temperature.

To overcome the difficulties related to the homogeneous assumption, Dunn [20] and Subramaniam and Mengüç [21] reported an inverse method using the Monte Carlo method with importance sampling with applications to *inhomogeneous* planar media. Unlike the traditional inverse method, the method described requires only one direct simulation but the optical thickness is either assumed to be known or determined from independent experiments. Moreover, as a statistically based method the Monte Carlo method requires to track a large number of photon bundles and hence large computer resources for a reasonable accuracy [14].

An alternative technique to measure the radiation properties of porous materials has been presented by Yamada, Kurosaki, and co-workers [22, 23]. First, Take-Uchi

et al. [22] presented a method to determine the extinction coefficient, the albedo and the back-scattering fraction factor of fiberglass batting. The albedo and the back-scattering fraction factor were estimated by heating an optically thick sample at 108^{o}C and measuring its normal emittance. The extinction coefficient was determined independently by transmittance measurements of a thinner sample. The analysis is based on the two-flux model and on the assumptions that the radiative properties do not depend on temperature and that the temperature in the medium is uniform. The albedo and the back-scattering fraction factor are determined using the least-square optimization technique. Further simplification has been presented more recently by Yamada and Kurosaki [23] who assumed an isotropic scattering phase function. In both cases, the authors used the fact that the emittance of an optically thick and isotropically scattering medium is independent of the optical thickness and depends only on the albedo and on the back-scattering fraction factor (=0.5 if isotropic scattering is assumed). Finally, the authors recommend the simplified method for highly scattering media rather than for absorbing media since the albedo is very sensitive to emittance which is larger for strongly absorbing media.

In the present study, spectral bi-directional measurements are used to identify radiation characteristics of fused quartz containing bubbles. Usually, spectral bi-directional measurements are performed for high porosity foams and fibrous media with negligible reflectivities at the interfaces. However, the samples under consideration have porosity around 10% and reflectivities at the fused quartz/surrounding interface cannot be neglected.

3. Experiments and Methodology

A. Experimental Setup

Figure 1 shows the experimental setup used to measure the spectral bi-directional transmittance and reflectance of the quartz samples containing bubbles and shows the path of the radiation from the radiation source to the detector. A radiation source is generated from a Fourier transform infrared spectrometer (FTS 60 A, Bio-Rad, Inc.) operating in the spectral range 1.5-25 μm. The source is distant from the spherical mirror SM1 by twice its focal distance and corresponds to a blackbody emission spectrum at 1300^{o}C emitting a radiation beam 7 mm in diameter. The diaphragm is located in the focal point of mirror SM2 and consists of four cylindrical holes of different radii R_A that determined the divergence half-angle θ_0 of the outcoming beam of the FTIR expressed as

$$\theta_0 = Arctan(\frac{R_A}{f_2}) \tag{3}$$

where f_2 is the focal distance of mirror SM2. For a good resolution one needs to reduce the divergence of the beam by reducing the radius of the diaphragm. However, this also reduces the energy of the signal. Thus, a compromise must be found between the energy of the signal leaving the FTIR and the resolution. The optimum diaphragm diameter was found to be $R_A = 2.7$ mm leading to a resolution of 2 cm^{-1} and a divergence half-angle $\theta_0 = 1.27^o$ [24].

The detection system consists of a spherical mirror collecting the transmitted radiation and concentrating it on a liquid nitrogen cooled MCT (HgCdTe) detector (Bio-Rad, Inc. model 997-0038) located at its focal point. The detection system is

mounted on a rotating arm enabling the measurement of the spectral bi-directional transmittance and reflectance in any arbitrary direction in the plane of incidence as shown in Figure 1. The rotation axis of the goniometer is passing in the plane of the incident face of the sample for reflectance measurements and in the plane of the other face for transmittance measurements. The entire system was purged with dry air to avoid infrared absorption by water vapor and carbon dioxide. The radiation emitted by the source is modulated and the detection is synchronized so that the radiation emitted by the sample and the surroundings are not measured.

The bi-directional transmittances and reflectances $T_{e,\lambda}(\theta)$ for normal incidence are defined by

$$T_{e,\lambda}(\theta) = \frac{I_\lambda(\theta)}{I_{0,\lambda} \mathrm{d}\omega_0} \tag{4}$$

where $I_\lambda(\theta)$ is the transmitted or reflected intensity in the θ-direction and $I_{0,\lambda}$ is the intensity of the collimated beam normally incident onto the sample within the solid angle $\mathrm{d}\omega_0 = 2\pi(1-cos\theta_0)$. The solid angle of detection is denoted $\mathrm{d}\omega_d = 2\pi(1-cos\theta_d)$ where θ_d is the detection angle measured experimentally as 0.19^o. The spherical mirror obstructs the incident beam and prevents the measurement of the spectral bi-directional reflectance for directions close to $\theta = 180^o$. To overcome this difficulty, the sample holder is rotated by an angle $\theta_a = 5^o$ (see Figure 2) enabling the measurement of specular reflection and is equivalent to reflectance measurements at 180^o with normal incidence if one assumes that the reflection is independent of the incident angle (for small angles) [25]. The same approach is used for the other directions of the quadrature scheme for which the sample holder obstruct the incident beam.

Finally, the reflection of the incident radiation by the sample holder can significantly affect the reflectance measurements, particularly for small diaphragms of the sample holder. The sample holder consists of two rigid plates having a circular diaphragm between which the sample is placed. Painting the sample holder with an absorbing black paint was not sufficient to minimize such a disturbance. Consequently, the sample holder including the front and back diaphragms were coated with soot particles by placing them in a combustion chamber where ethylene and oxygen burned with an excess of oxygen. Then, the measurements of the sample holder emissivity has been measured and indicate that it behaves as a blackbody across the entire spectral range of the detector. Doermann [24] also showed that assuming a uniform incident radiation intensity may not be valid if the diaphragm placed in front of the sample is too large. Therefore, a compromise should be found in order to find the largest possible diaphragm that would give the largest radiation intensity and signal to noise ratio possible while satisfying the assumption of uniform incident intensity used as a boundary condition in the inversion scheme. The optimum diaphragm diameters was found to be 35 mm leading to a sample thickness to diaphragm diameter ratio between 1/12 and 1/4. In the inversion procedure the radiative transfer equation is solved assuming that the radiation intensity profile of the incident beam falling on the sample is uniform [see boundary condition expressed by Equation (7)]. In general, the intensity profile assumes a bell shape with a plateau in the center and a sharp decrease at the edges. The uniformity of the radiation intensity falling onto the sample, i.e., the extent of the plateau in the center of the beam depends both on the spectrophotometer aperture and the size of the diaphragm placed in front of the

sample.

B. Sample Description

Fused quartz samples containing bubbles have been prepared and analyzed. The fused quartz is the Osram Sylvania SG25 Lighting grade containing a negligible hydroxyl content with a maximum of 5 ppm. Samples were cut with a diamond saw from a large piece of quartz collected during the shutdown of an industrial furnace in which the fused quartz is electrically heated in an inert atmosphere of helium and hydrogen. The samples were then ground with a diamond wheel and polished with silicon carbide papers of different grids. Desirable finish was achieved using a rotating cork belt. The samples were cleaned with a 1:1 mixture of sulfuric acid and hydrogen peroxide at 30% for 10 minutes, followed by a 10 minutes rinse in de-ionized water. The samples were finally dried by blowing them with ultra-pure nitrogen. Five samples of different thicknesses (3, 5, 5.6, 6, and 9 mm) have been studied, all having an average void fraction of $0.094 \pm 16\%$ and a 5 cm $\times$ 5 cm cross-section. The samples are cut relatively thin so that (1) the width to thickness ratio is large enough to assure one-dimensional radiative transfer, and (2) the transmitted signal to noise ratio is large enough for the measurements to be meaningful. Due to the small thickness, the sample thickness to average bubble diameter ratio is small and inhomogeneities exist. However, the cross-sectional area of the incident beam is large (about 35 mm) compared with the average cross-sectional area of the bubbles. Therefore, the radiation encounters numerous bubbles as it passes through the sample leading to an averaging effect that smoothes out the inhomogeneities as confirmed by Baillis and

Sacadura [18]. In other words, the radiation characteristics κ_λ, σ_λ, β_λ and $\Phi(\theta)$ recovered from the bi-directional transmittance and reflectance measurements vary little with the sample thickness, i.e., the local inhomogeneities do not affect the results of the inversion and the homogeneous assumption is valid.

Figure 3 shows a photograph of a typical 3 mm thick sample of 5 cm x 5 cm cross section. The bubble size distribution was determined from the analysis of more than 120 images of individual bubbles. As one can see in Figures 3, the bubbles are spherical in shape, randomly distributed, and their size distribution is relatively uniform as illustrated in Figure 4. The average bubble radius is 1.14 mm. The fact that bubbles are randomly distributed assures that radiation characteristics of the medium are independent of the azimuthal angles and that bidirectional transmittances are symmetric with respect to the incident direction. Even though micrographs were taken from two different samples, all the samples were assumed to have the same bubble size distribution and void fraction since the samples were prepared from the same large piece of glass.

C. Inverse Method

The radiation characteristics of the samples are determined by an inverse method. The inversion consists of determining iteratively the radiation characteristics that minimize the sum F of the quadratic difference between the measured and calculated bi-directional transmittance and reflectance over the n discrete directions θ_i. At each wavelength λ, F is given by

$$F[\omega_\lambda, \beta_\lambda, \Phi(\theta_i)] = \sum_{i=1}^{n} [T_{t,\lambda}(\theta_i) - T_{e,\lambda}(\theta_i)]^2 \tag{5}$$

The function $F[\omega_\lambda, \beta_\lambda, \Phi(\theta_i)]$ is minimized by Gauss linearization method, i.e., by setting to zero the derivatives of F with respect to each of the unknown parameters [26].

The theoretical spectral transmittances and reflectances were computed by solving the radiative transfer equation based on the following assumptions: (1) the radiation transfer is assumed to be one-dimensional, (2) azimuthal symmetry prevails, (3) the medium emission term can be disregarded due to the radiation modulation and the phase sensitive detection, (4) the medium is homogeneous, and (5) the effect of polarization on the bi-directional reflectance is not considered.

Solution of the RTE is obtained by using the discrete ordinates method in the n directions of the quadrature scheme. Under the above assumptions, the discretized one-dimensional RTE in the direction θ_i can be expressed as the following system of n partial differential equations (one for each direction)

$$\mu_i \frac{\partial I_\lambda(\tau_\lambda, \mu_i)}{\partial \tau_\lambda} = -I_\lambda(\tau_\lambda, \mu_i) + \frac{\omega_\lambda}{2} \sum_{j=1}^{n} w_j \left[\Phi(\mu_j, \mu_i) I_\lambda(\tau_\lambda, \mu_j) + \Phi(-\mu_j, \mu_i) I_\lambda(\tau_\lambda, -\mu_j)\right] \tag{6}$$

where $\mu_i = cos\theta_i$ is the cosine director, τ_λ is the spectral optical coordinate, and w_i is a weighting factor associated with the ordinate direction θ_i. The weighting factors w_i depend on the quadrature scheme [27] and are listed in Table 1 for the quadrature consisting of 24 directions and corresponding to a half angle θ_0 of 1.27^o. The quadrature is a combination of two Gauss quadratures that allows for a concentration of ordinates in the neigborhood of the normal direction suitable for forward scattering media. The boundary conditions are obtained by assuming that the interfaces are optically smooth, i.e., surface roughness is small compared with the wavelength of

radiation and reflections are specular. Indeed, the void fraction is relatively small and the effect of open bubbles at the sample surface can be neglected. Then, the boundary conditions associated with the RTE for normal incident radiation are given by

$$I_\lambda(0,\mu_j) = r_{21} I_\lambda(0,-\mu_j) + (n_\lambda^c)^2 (1-r_{12}) \delta_{\mu_0,\mu_j} I_\lambda(0,\mu_0) \qquad \mu_j > 0 \quad (7)$$

$$I_\lambda(\tau_{\lambda,L},\mu_j) = r_{21} I_\lambda(\tau_{\lambda,L},-\mu_j) \qquad \mu_j < 0 \quad (8)$$

where r_{12} and r_{21} are the interface reflectivities as shown in Figure 5, and $\tau_{\lambda,L}$ is the optical thickness of the entire sample, i.e., $\tau_{\lambda,L} = \tau_\lambda(x = L)$. The Kronecker's delta function is denoted δ_{μ_0,μ_j} (= 1 if $\mu_j = \mu_0$ and =0 otherwise) with $\mu_j = cos(\theta_j)$ and $\mu_0 = 1$ for normal incidence.

In general, reflectivities are determined from the complex index of refraction [27]. In spectral regions where the complex part is negligible (weakly absorbing materials), reflectivities at the interface r_{12} can be determined from the Fresnel's equation [1,27],

$$r_{12} = \frac{1}{2}\left[\frac{sin^2(\theta-\chi)}{sin^2(\theta+\chi)} + \frac{tan^2(\theta-\chi)}{tan^2(\theta+\chi)}\right] \quad (9)$$

where θ is the angle of incidence betwen the normal and the incident radiation onto the surface. The angle of refraction of the radiation from within the layer onto the back surface of the slab is denoted χ. For normal incident radiation, the external surface reflectivity (r_{12}) simplifies as [1,27]

$$r_{12} = \frac{(n_\lambda^c - 1)^2}{(n_\lambda^c + 1)^2} \quad (10)$$

Moreover, due to the presence of a large number of scatterers (bubbles) in the condensed phase layer (medium 2), the radiation field inside the layer does not reach the interface normally. Thus, the internal surface reflectivitivity r_{21} is also given by

Equation (9) but with $\theta = \chi_j$ the incident angle of radiation coming from the medium and $\chi = \theta_j$ the refraction angle at the interface. The angles χ_j and θ_j are related by Snell's law

$$n_\lambda^c sin\chi_j = sin\theta_j \tag{11}$$

Thus, the reflected and transmitted intensity used to calculate the transmittance and reflectance required in the identification processus are given, respectively, by

$$I_\lambda(0,\mu_i) = r_{12}\delta_{\mu_0,-\mu_i} I_\lambda(0,\mu_0) + \left(\frac{1}{n_\lambda^c}\right)^2 (1-r_{21}) I_\lambda(0,\mu_j) \qquad \mu_i < 0 \tag{12}$$

$$I_\lambda(\tau_{\lambda,L},\mu_i) = \left(\frac{1}{n_\lambda^c}\right)^2 (1-r_{21}) I_\lambda(\tau_{\lambda,L},\mu_j) \qquad \mu_i > 0 \tag{13}$$

where $\mu_j = cos\theta_j$ is obtained from Snell's law. The scattering phase function was assumed to follow the Henyey-Greenstein normalized form involving only the asymmetry factor g and expressed as [1]

$$\Phi_\lambda(\theta) = \frac{1-g^2}{[1+g^2-2gcos\theta]^{3/2}} \tag{14}$$

The shape coefficient g can vary between 0 (isotropic scattering) and ± 1 (+ for strictly forward scattering and - for backward scattering).

Finally, the space is discretized in order to numerically solve the above system of partial differential equations with the associated boundary conditions [Equations (6) to (8)] by the finite volume method [19, 24]. The results obtained by the discrete ordinates method may depend strongly on the number of directions and on the spatial discretizations chosen. In order to reduce the computational time and still provide adequately accurate results grid sensitivity studies have been performed. The numerical results were shown to be independent of the number of control volumes considered and

190 control volumes in each ordinate direction were sufficient to obtain a converged solution.

D. Infrared Optical Constants of Fused Quartz

The index of refraction of fused quartz in the spectral range of the infrared detector ($0.2\mu\text{m} \leq \lambda \leq 15\mu\text{m}$) is necessary for determining the reflectivity at the glass sample/surrounding interface used in the boundary conditions. Different correlations for the real part of the complex index of refraction of fused quartz as a function of wavelength have been suggested in the literature [28–30] for different spectral regions. Rodney and Spindler [28] suggested an expression for n_λ^c over the spectral range from 0.347 to 3.508 μm at 31^{o}C while Tan and Arndt [30] proposed another equation in the spectral region from 1.44 to 4.77 μm at temperatures ranging from 23.5 to 481^{o}C. Over the spectral range from 0.21 to 3.71 μm at 20^{o}C, Malitson [29] fitted experimental data with the following three-term Sellmeier equation,

$$(n_\lambda^c)^2 = 1 - \frac{0.6961663\lambda^2}{\lambda^2 - (0.0684043)^2} + \frac{0.4079426\lambda^2}{\lambda^2 - (0.1162414)^2} + \frac{0.8974794\lambda^2}{\lambda^2 - (9.896161)^2} \qquad (15)$$

Moreover, Tan [31] confirmed the validity of Equation (15) for wavelengths up to 6.7 μm. Therefore, due to its wide range of validity (from 0.21 to 6.7 μm) at room temperature, Equation (15) is used in the present study.

E. Experimental Uncertainty

In the case of bi-directional measurement, experimental uncertainty are mainly due to the alignment [24]. To assess the experimental uncertainty, four different alignements were performed and spectral bi-directional transmittances and reflectances were meas-

ured for each sample. The average spectral transmittance or reflectance in direction θ_i and wavelength λ denoted $\bar{T}_\lambda(\theta_i)$ along with the mean square deviations Δ_i have been computed as

$$\bar{T}_\lambda(\theta_i) = \frac{1}{4}\sum_{k=1}^{4} T_{k,\lambda}(\theta_i) \tag{16}$$

$$\Delta_i = \frac{1}{\bar{T}_\lambda(\theta_i)}\sqrt{\frac{1}{3}\sum_{k=1}^{4}\left(T_{k,\lambda}(\theta_i) - \bar{T}_\lambda(\theta_i)\right)^2} \tag{17}$$

Then, the resulting average spectral bi-directional transmittances and reflectances were used as input parameters to the inversion algorithm. The experimental error on the measured transmittances and reflectances depends on the ordinate directions and on the wavelength. Indeed, the signal to noise ratio decreases as one moves away from the incident direction corresponding to $\theta_i = 0.0^o$.

4. Results and Discussion

The input parameters for the inverse method are the (i) sample thickness L, (ii) the ordinate directions θ_i and the associated weighting factors w_i, and (iii) the complex index of refraction of fused quartz. The radiation characteristics retrieved from the inversion are the single scattering albedo ω_λ, the extinction coefficient β_λ, and the Henyey-Greenstein asymmetry factor g. Then, the absorption and scattering coefficients can be determined from

$$\kappa_\lambda = \beta_\lambda(1-\omega_\lambda) \qquad \text{and} \qquad \sigma_\lambda = \beta_\lambda\omega_\lambda \tag{18}$$

This section presents the radiation characteristics of fused quartz containing bubbles obtained by inverse method. It aims at discussing in details the validity of the results

and their sensitivity to input parameters as well as providing physical explanations to the results.

A. Discussion of the Inverse Method

In order to retrieve the radiation characteristics of the samples, the RTE and the associated boundary conditions were solved in 24 different angles of ordinate directions and for 200 different wavelengths in the spectral region from 1.67 μm to 3.5 μm. Since the set of equations solved by the inverse method is ill posed, a small uncertainty in the experimental data could lead to large variations and errors in the recovered results. Therefore, it is essential to perform a sensitivity study to assess the effect of small changes in the input parameters [32]. To do so, uncertainty on the real (n_λ^c) part of the index of refraction of fused quartz were estimated to be 2% while the uncertainty on the sample thickness L is estimated to be 2 %. It was shown that error on the sample thickness L has negligible influence on the results of the inverse method. However, an uncertainty of 2% in n_λ^c leads to a similar uncertainty in the retrieved extinction coefficient, single-scattering albedo, and asymmetric factor g but is still acceptable since experimental data for n_λ^c appear to be very accurate and highly reproducible as discussed previously. The difference of reflectivities calculated from Equation (9) neglecting the absorption index k_λ^c and these obtained without neglecting the absorption index [27] remains less than 4.5×10^{-2} % and all the retrieved parameters vary by less than 10^{-6}% for all the samples and wavelengths in the range from 1.67 μm to 3.5 μm. This confirms that the absorption index k_λ^c can be neglected in the calculation of reflectivities and that Equation (9) is valid for fused quartz in

the spectral range of interest.

Due to the weak signal transmitted in directions far from the incident direction, only eight forward directions and three backward directions have been used. To verify the good behavior of the model and the validity of the results, the influence of the number of ordinate directions used for the inversion has been investigated. Figure 6 illustrate the effect of the number of ordinate directions for the single-scattering albedo of the 5.5 mm thick sample. It indicates that unlike the number of backward directions considered, the number of forward directions considered has significant effect on the retrieved parameters. The study shows that at least three angles θ_i are needed in the forward direction in order to have convergence of the inversion algorithm. The results were shown to be independent of the number of ordinate directions if at least five different angles θ_i close to $\theta = 0^o$ (forward) and two near $\theta = 180^o$ (backward) were considered. The number of wavelengths for which the inversion algorithm converges increases with the number of directions accounted for.

Similarly, sensitivity study for the initial values taken for β_λ, ω_λ, and g has been carried out. In brief, the inverse algorithm converges always to the same solutions for different sets of initial estimates of the radiation characteristics.

Moreover, beyond wavelengths of 4.5 μm fused quartz is strongly absorbing, thus reducing the magnitude of the transmitted signal and increasing the experimental uncertainty. The measurements were performed for wavelengths between 1.67 μm and 3.5 μm. The lower limit corresponds to the limit of the detector while for wavelengths larger than 3.5 μm the inverse algorithm could not converge for certain samples.

Furthermore, the difference between $r_{12}(0^o)$ and $r_{12}(5^o)$ remains less than 3.10^{-3}

% for wavelengths between 1.67 μm and 3.5 μm. Thus, the reflection can be assumed to be independent of the angle for small angles and the technique described in Figure 2 can be used to measure the reflectance at 180^o.

Finally, it was not necessary to measure spectral directional-hemispherical transmittance and reflectance as suggested by Baillis *et al.* [17, 18], owing to the good behavior of the inversion algorithm in terms of convergence and sensitivity.

B. Analysis of the Experimental Results

Figure 7 shows the extinction coefficient, the single-scattering albedo, and the Henyey-Greenstein asymmetric factor as a function of wavelength retrieved for the different samples. One can see that the retrieved characteristics do not vary significantly with the sample thickness larger than 3 mm which confirms the good behavior of the inversion algorithm using Equations (6) through (15). However, the 3 mm thick sample has a spectral extinction coefficient much larger than that of the other samples. This can be explained by the fact that the sample may be too thin to be treated as homogeneous or that the effect of open bubbles at the sample surface cannot be neglected for thin samples, i.e., the interfaces cannot be treated as optically smooth. Similar observations have been reported by Hale and Bohn [14] for open-cell reticulated alumina foams.

Based on the above remarks, the radiation characteristics retrieved for the 3 mm thick sample have not been considered. The spectral data for the four other samples have been averaged at each wavelength and are shown in Figure 8 along with the associated standard deviation. The retrieved radiation characteristics for the 9

mm thick sample deviate slightly from those obtained with 5, 5.6, and 6 mm thick samples for single-scattering albedo and asymmetry factor. The maximum standard deviation is observed for the single-scattering albedo but does not exceed 14%. The single-scattering albedo ranges between 0.06 and 0.11 indicating that the radiation transfer is dominated by absorption by the fused quartz matrix. It also indicates that even for a small void fraction of about 10%, scattering caused by the presence of bubbles contributes between 6 and 11% to the total extinction coefficient. The single-scattering albedo is expected to be larger for glass samples containing smaller bubbles and thus having larger interfacial area.

The absorption and scattering coefficients were computed from Equation (18) and are presented in Figure 9. The scattering coefficient is relatively small due to the small void fraction and the relatively large bubble size resulting in a small interfacial surface area. Indeed, scattering is caused by the reflection and diffraction of the radiation at the gas/fused quartz interface and should strongly depend on the interfacial area. Moreover, the absorption coefficient presents a peak around wavelength of 2.7 μm. It is attributed to hydroxyl groups present as impurities in the fused quartz. Indeed, O-H stretching vibration present a maximum at about 2.72 μm and is believed to consist of four Gaussian components corresponding to different O-H bonding configurations in the SiO_2 matrix [33]. The absorption by the impurities such as hydroxyl groups is particularly noticeable around 2.7 μm since the complex part of the index of refraction of fused quartz is very small over the spectral region from 0.2 to 4.5 μm. One could also mention that carbon dioxide and water vapor present a strong absorption bands at 2.7 μm [27] and could be entrapped in the bubbles as commonly

observed in glass manufacturing [34]. However, the industrial process used to manufacture the fused quartz under consideration consists of heating pure silicon dioxide electrically in an inert atmosphere of helium and hydrogen [35]. Moreover, analysis of gas bubble content indicates that bubbles contain mainly carbon monoxide, along with helium, and hydrogen [35]. These gases do not absorb around 2.7 μm [27] and should not influence the radiation characteristics of fused quartz containing bubbles. Consequently, hydroxyl (OH) groups are solely responsible for the absorption peak around 2.72 μm. Beside the absorption peak around 2.7 μm, the retrieved values of the absorption coefficient are larger than that computed from the optical properties of dense fused quartz reported in the literature. Additional absorption could be due to trapping of radiation by successive inter-reflections within the bubbles caused by the curvature of the bubble surface. However, the optical properties of fused quartz in the spectral region from 1.67 to 3.5 μm depend strongly on the impurity concentration and therefore no quantitative conclusion can be drawn.

Finally, the experimental error computed from Equation (17) is conservatively estimated to be 9%, i.e., $\Delta_i < 9\%$ in the normal direction and to 25% at $\theta_i = 3.32^o$. The computed spectral transmittances and reflectances fall systematically within the experimental uncertainty error bars for all samples and directions except for $\theta = 180^o$. For example, Figure 10 compares the experimental transmittance obtained with the 5.6 mm thick sample for typical directions 1 and 3 ($\theta_i = 0^o$ and 3.32^o, respectively) with those obtained numerically by solving the RTE using the discrete ordinates method and the average spectral extinction coefficient, the single-scattering albedo, and the asymmetry factor obtained by inverse method. One can see that the com-

puted spectral transmittance falls within the experimental uncertainty error bars representing the interval $[T_{e,\lambda}(\theta_i) - \Delta_i, T_{e,\lambda}(\theta_i) + \Delta_i]$.

5. Conclusions

The radiation characteristics of fused quartz containing bubbles have been measured experimentally. So far, spectral bidirectional transmittance and reflectance measurements have been performed for high porosity material such as foam and fibrous media. In this work, the porosity is approximately 10% and reflectivities at the interface have been taken into account assuming smooth interfaces. To experimentally study the influence of bubbles on the radiation characteristics of fused quartz, five different samples with thickness comprised between 3 mm and 10 mm were considered. Experimentally, it has been established that

- The assumption of one-dimensional radiation transfer appears to be appropriate for samples thicker than 3 mm.

- Inconsistencies in the retrieved radiation characteristics appear for the 3 mm thick sample. They can be attributed to the fact that the homogeneous assumption may not be valid for such thin samples and/or the effect of open bubbles at the sample surface can no longer be neglected.

As far as the effect of bubbles on the radiation characteristics of fused quartz is concerned, the following conclusions can be drawn:

- The presence of the bubbles seems to increase the extinction coefficient due to the scattering of the radiation at the bubble glass interface in the spectral range

from 1.67 μm to 3.5 μm. For a void fraction of about 10%, scattering caused by the presence of bubbles contributes between 6 and 11% to the total extinction coefficient.

- The scattering phase function of quartz containing bubbles is directed strongly forward as predicted by the model discussed by Viskanta and co-workers [11–13]. The Henyey-Greenstein phase function appears to be appropriate to represent the scattering of semitransparent media containing bubbles.

ACKNOWLEDGEMENTS

This work was supported in part by the U.S. Department of Energy/ Glass Industry/ Argonne National Laboratory/ University collaborative research project. The authors are indebted to Messrs. William Anderson and Richard Marlor of Osram Sylvania for providing the fused quartz samples and for their helpful discussions and exchanges of information.

References

1. M. F. Modest, *Radiative Heat Transfer*, McGraw-Hill, New York, NY (1993).
2. D. Baillis and J.-F. Sacadura, "Thermal radiation properties of dispersed media: theoretical prediction an experimental characterization", *Journal of Quantitative Spectroscopy & Radiative Transfer* **67**, 327–363 (2000).
3. J. Kuhn, H.-P. Ebert, M.C. Arduini-Schuster, D. Büttner, and J. Fricke, "Thermal transport in polystyrene and polyurethane foam insulations", *International Journal of Heat and Mass Transfer* **35**, 1795–1801 (1992).

4. G. Eeckhaut and A. Cunningham, "The elimination of radiative heat transfer in fine celled PU rigid foams", *Journal of Cellular Plastics* **32**, 528–552 (1996).

5. M. Schuetz and L. Glicksman, "A basic study of heat transfer through foam insulation", *Journal of Cellular Plastics* **20**, 114–121 (1984).

6. L.R. Glicksman, M. Schuetz, and M. Sinofsky, "Radiation heat transfer in foam insulation", *International Journal of Heat and Mass Transfer*, **30**, 187–197 (1987).

7. L.R. Glicksman, A.L. Marge, and J.D. Moreno, "Radiation heat transfer in cellular foam insulation", in *28th National Heat Transfer Conference and Exhibition. San Diego, CA, USA. HTD Vol. 203, Developements in Radiative Heat Transfer* (1997), pp. 45–54, ASME.

8. R. Viskanta and M. P. Mengüç, "Radiative transfer in combustion system", *Progress in Energy and Combustion Sciences* **13**, 97–160 (1987).

9. L.A. Dombrovsky, *Radiation Heat Transfer in Disperse Systems*, Begell House, New York, NY (1996).

10. M. Rubin, "Optical properties of soda-lime silicate", *Solar Energy Materials* **12**, 275–288 (1985).

11. L. Pilon and R. Viskanta, "Radiation characteristics of glass containing bubbles", *Journal of the American Ceramic Society* **86**, 1313–1320 (2003).

12. A. G. Fedorov and R. Viskanta, "Radiative transfer in a semitransparent glass foam blanket", *Physics and Chemistry of Glasses* **41**, 127–135 (2000).

13. A. G. Fedorov and R. Viskanta, "Radiative characteristics of glass foams", *Journal of the American Ceramic Society* **83**, 2769–2776 (2000).

14. M. J. Hale and M. S. Bohn, "Measurement of the radiative transport properties of reticulated alumina foams", in *Proceedings of the ASME/ASES Joint Solar Engineering Conference*, A. Kirkpatrick and W. Worek, Eds., New York, NY (1993), pp. 507–515, ASME.

15. T. J. Hendricks and J. R. Howell, "Absorption/scattering coefficients and scattering phase functions in reticulated porous ceramics", *Journal of Heat Transfer* **118**, 79–87 (1996).

16. D. Baillis, M. Raynaud, and J.-F. Sacadura, "Determination of spectral radiative properties of open-cell foam: model validation", *Journal of Thermophysics and Heat Transfer* **14**, 137–143 (2000).

17. D. Baillis, M. Arduini-Schuster, and J.-F. Sacadura, "Identification of spectral radiative properties of polyurethane foam from hemispherical and bi-directional transmittance and reflectance measurements", in *Proceedings of the 3rd International Symposium on Radiation Transfer*, M. P. Mengüc and N. Selcuk, Eds. , Begell House, Inc., New York (2001), pp. 474–482.

18. D. Baillis and J.-F. Sacadura, "Identification of polyurethane foam radiative properties - influence of transmittance measurements number", *Journal of Thermophysics and Heat Transfer* **16**, 200–206 (2002).

19. L. M. Moura, *Identification des propriétés radiatives des matèriaux semi-transparent diffusants en situation de non-symmetrie azimutale du champ radiatif*, PhD thesis, Institut National des Sciences Appliquées de Lyon, France, Lyon, France (1998).

20. W. L. Dunn, "Inverse Monte Carlo analysis", *Journal of Computational Physics* **41**, 154–166 (1981).

21. S. Subramaniam and M. P. Mengüç, "Solution of the inverse radiation problem for inhomogeneous and anisotropically scattering media using a Monte Carlo technique", *International Journal of Heat and Mass Transfer* **14**, 253–266 (1991).

22. Take-Uchi, Y. Kurosaki, T. Kashiwagi, and J. Yamada, "Determination of radiation properties of porous media by measuring emission", *JSME International Journal* **31**, 581–585 (1988).

23. J. Yamada and Y. Kurosaki, "Estimation of a radiative property of scattering and absorbing media", *International Journal of Thermophysics* **18**, 547–556 (1997).

24. D. Doermann, *Modélisation des transferts thermiques dans des matériaux semi-transparents de type mousse à pores ouverts et prédiction des propriétés radiatives*, PhD thesis, Institut National des Sciences Appliquées de Lyon, France (1995).

25. V.P. Nicolau, *Identification des propriétés radiatives des matèriaux semi-transparent diffusants*, PhD thesis, Institut National des Sciences Appliquées de Lyon, France (1994), (94 ISAL 0001.

26. J.V. Beck and K. J. Arnold, *Parameter estimation in engineering and science*, John Wiley & Sons, New York, NY (1977).

27. R. Siegel and J.R. Howell, *Thermal radiation heat transfer - Third Edition*, Hemisphere Publishing Co., New York, NY (1992).

28. W.S. Rodney and R.J. Spindler, "Index of refraction of fused quartz for ultraviolet, visible, and infrared wavelengths", *Journal of the Optical Society of America*

44, 677–679 (1954).

29. I.H. Malitson, "Interspecimen comparison of the refractive index of fused silica", *Journal of the Optical Society of America*, **55**, 1205–1209 (1965).

30. C.Z. Tan and J. Arndt, "Temperature dependence of refractive index of glass SiO_2 in the infrared wavelength range", *Journal of Physics and Chemistry of Solids* **61**, 1315–1320 (2000).

31. C.Z. Tan, "Determination of refractive index of silica glass for infrared wavelengths by ir spectroscopy", *Journal of Non-Crystalline Solids* **223**, 158–163 (1998).

32. M. Raynaud, "Strategy for the experimental design and the estimation of parameters", *High Temperatures-High Pressures* **31**, 1–15 (1999).

33. V.G. Plotnichenko, V.O. Sokolov, and E.M. Dianov, "Hydroxyl groups in high-purity silica glass", *Journal Non-Crystalline Solids* **261**, 186–194 (2000).

34. R. G. C. Beerkens, "The role of gases in glass melting processes", *Glastechnische Berichte* **71**, 369–380 (1995).

35. R. Marlor and W. Anderson, Osram Sylvania Inc., Glass Technologies Headquarters, Exeter, NH 03833, USA. Personal communication (July 2002).

Figure Captions

Figure 1. Schematic of the experimental apparatus used to measure the spectral transmittance and reflectance.

Figure 2. Reflectance measurements in the directions between 170^o and 180^o with θ_a=5^o.

Figure 3. Digital photograph of a 3 mm thick fused quartz sample containing bubbles (porosity $\approx$ 10%).

Figure 4. Bubble size distribution obtained from more than 120 images of individual bubbles.

Figure 5. Schematic of the idealized liquid layer containing bubbles and the coordinate system.

Figure 7. Retrieved extinction coefficient, single-scattering albedo and Henyey - Greenstein asymmetry factor determined by inverse method for each samples.

Figure8. Average retrieved extinction, single-scattering albedo and Henyey - Greenstein asymmetry factor by inverse method for each samples and their standard deviation.

Figure 9. Average retrieved absorption (top) and scattering coefficients (bottom).

Figure 10. Comparison between the average measured spectral transmittance with error bars corresponding to $T_{e,\lambda}(\theta_i) \pm \Delta_i$ and the numerical results obtained with the averaged retrieved radiation characteristics for (top) $\theta_i = 0^o$ and $\Delta_i = 9\%$, and (bottom) $\theta_i = 3.32^o$and $\Delta_i = 25\%$.

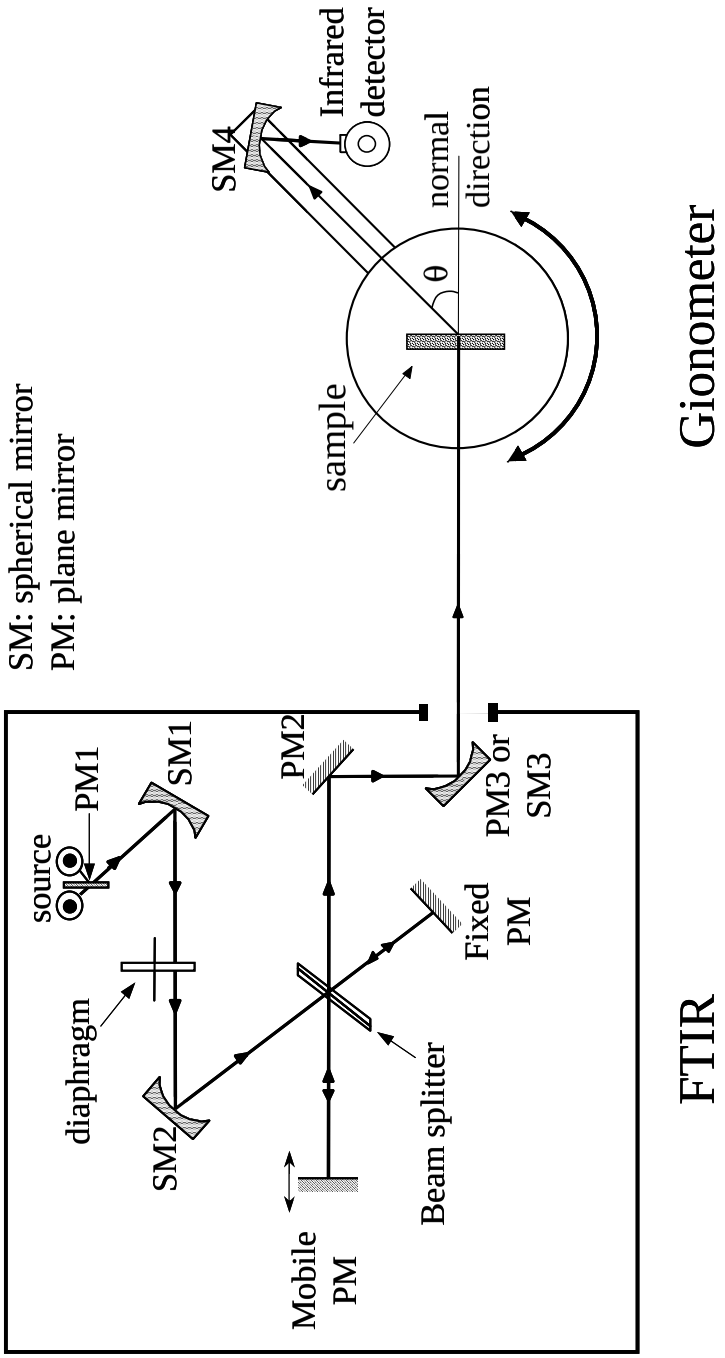

Fig. 1. Schematic of the experimental apparatus used to measure the spectral transmittance and reflectance.

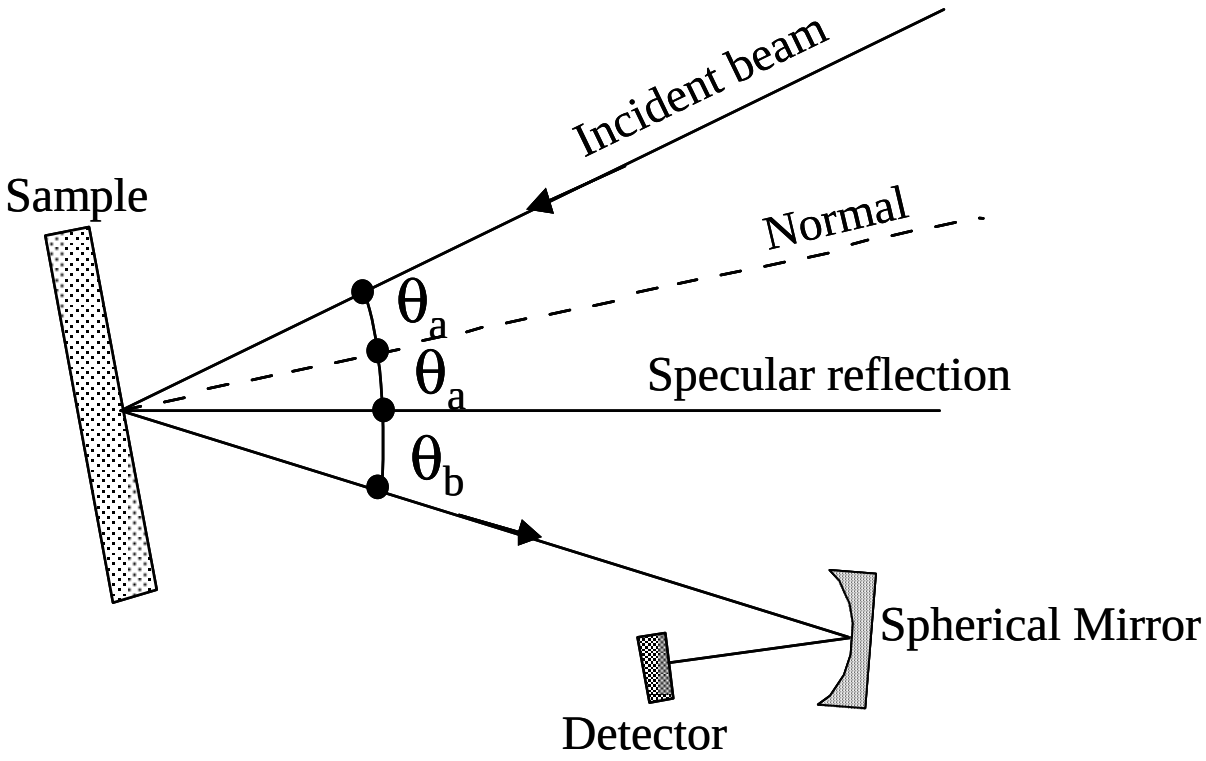

Fig. 2. Reflectance measurements in the directions between 170^o and 180^o with θ_a=5^o.

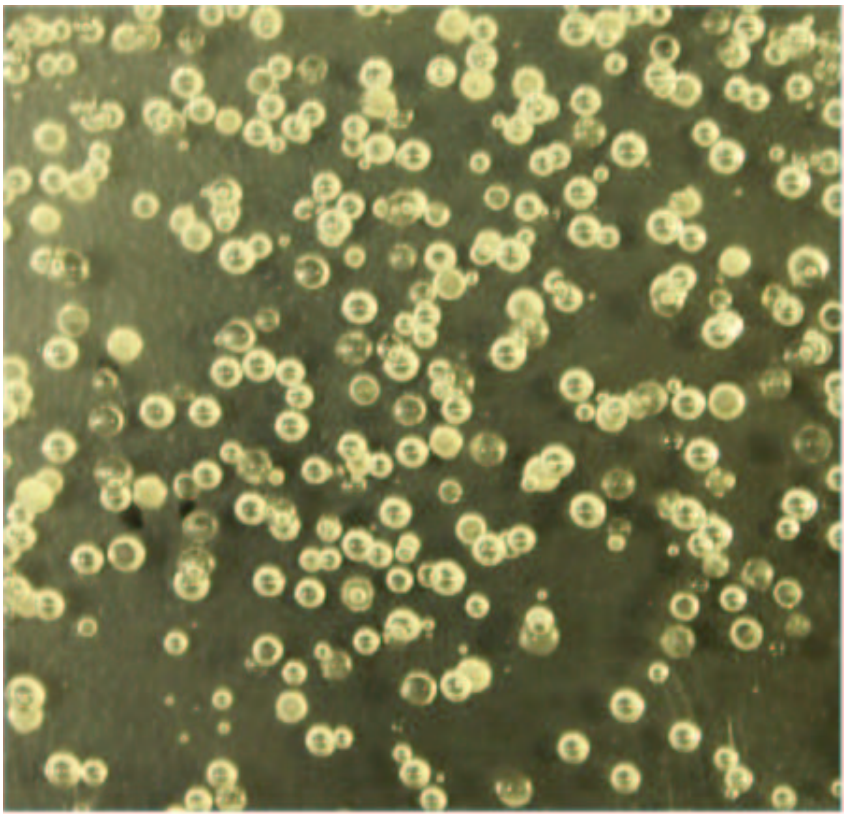

Fig. 3. Digital photograph of a 3 mm thick fused quartz sample containing bubbles (porosity $\approx 10\%$).

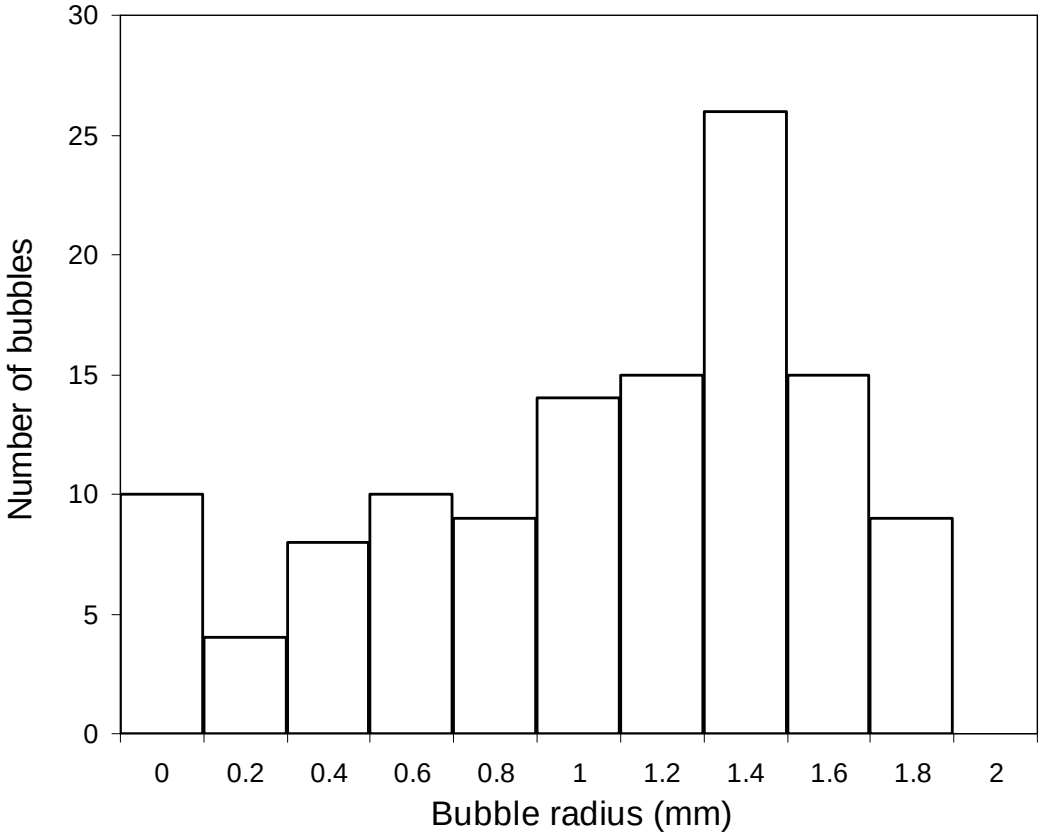

Fig. 4. Bubble size distribution obtained from more than 120 images of individual bubbles.

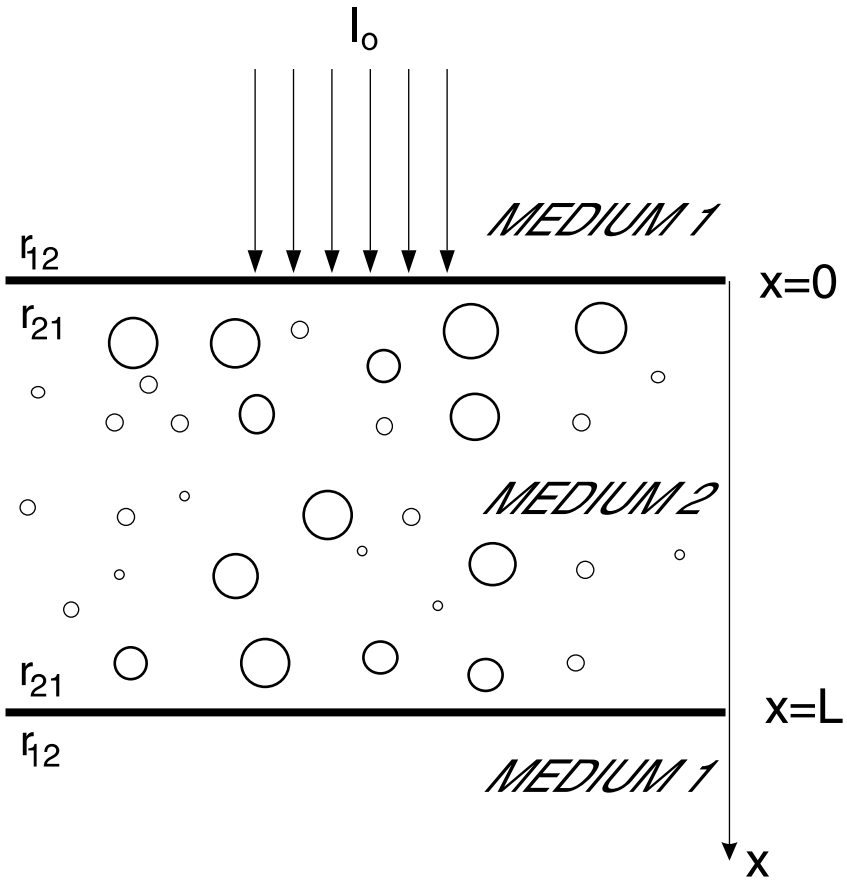

Fig. 5. Schematic of the idealized liquid layer containing bubbles and the coordinate system.

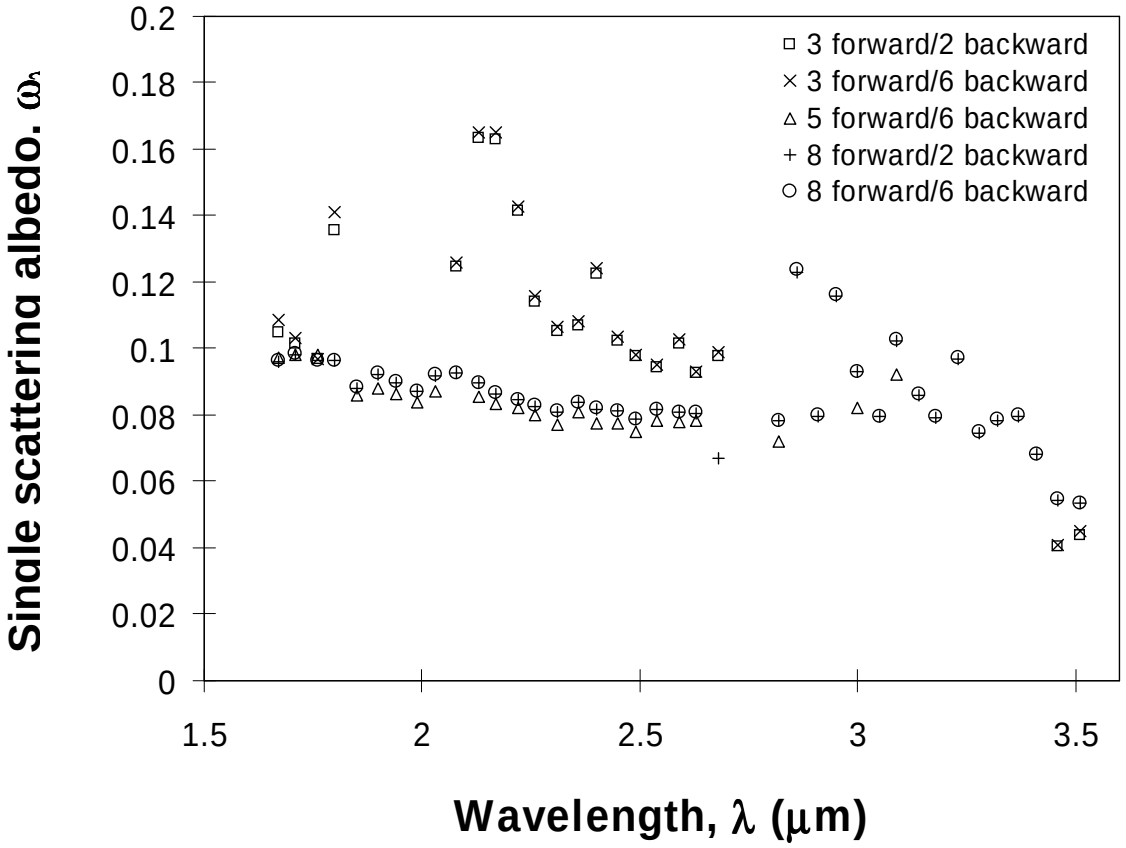

Fig. 6. Illustration of the effect of the number of directions accounted for on the results of the inversion algorithm for spectral single-scattering albedo of the 5.6 mm thick sample.

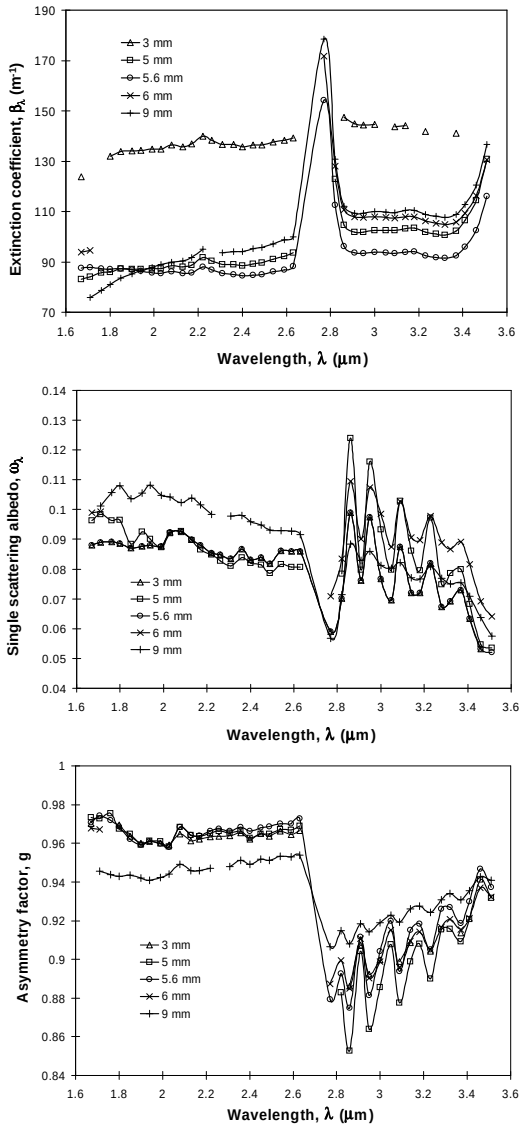

Fig. 7. Retrieved extinction coefficient, single-scattering albedo and Henyey - Greenstein asymmetry factor determined by inverse method for each samples.

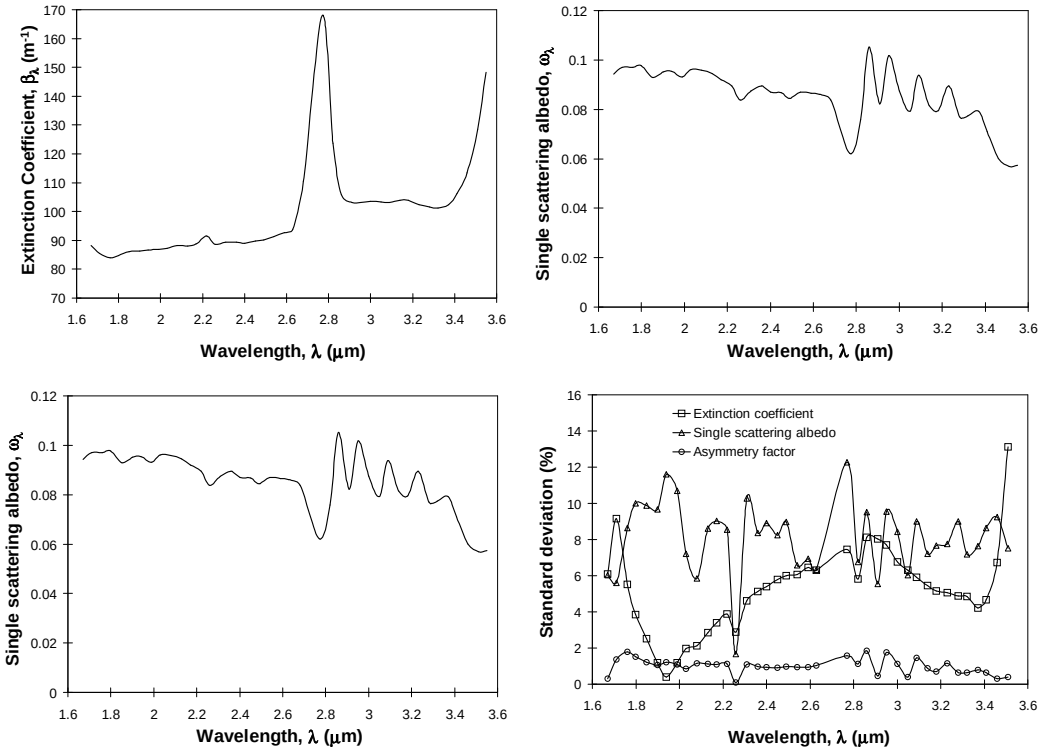

Fig. 8. Average retrieved extinction, single-scattering albedo and Henyey - Greenstein asymmetry factor by inverse method for each samples and their standard deviation.

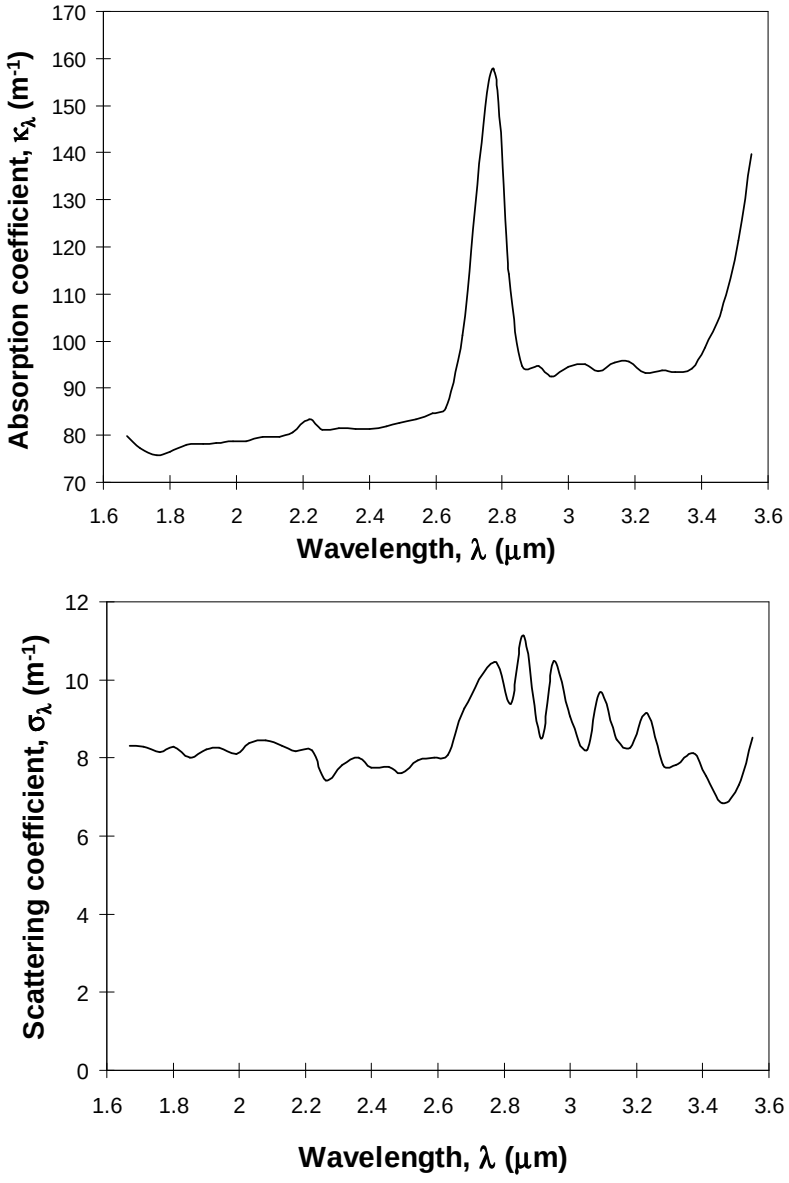

Fig. 9. Average retrieved absorption (top) and scattering coefficients (bottom).

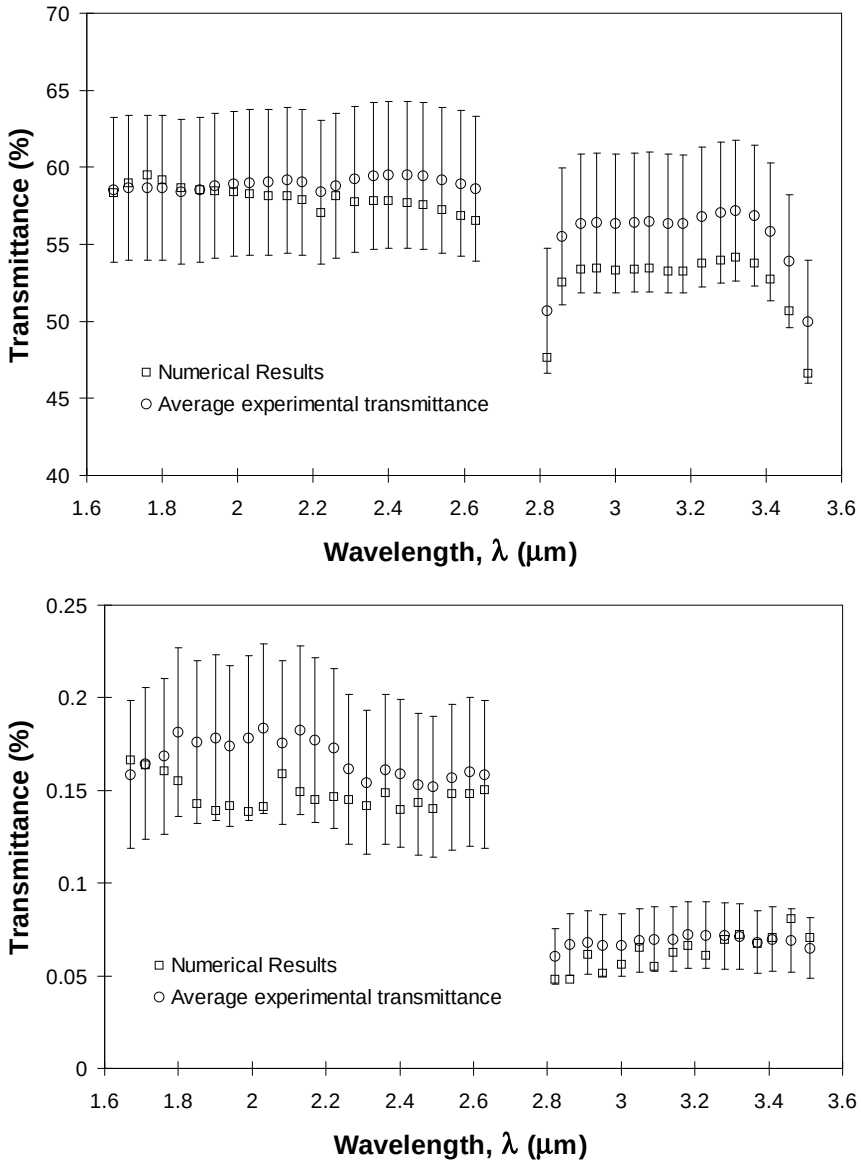

Fig. 10. Comparison between the average measured spectral transmittance with error bars corresponding to $T_{e,\lambda}(\theta_i) \pm \Delta_i$ and the numerical results obtained with the averaged retrieved radiation characteristics for (top) $\theta_i = 0^o$ and $\Delta_i = 9\%$, and (bottom) $\theta_i = 3.32^o$and $\Delta_i = 25\%$.

Table 1. 24 directions and corresponding weighting factors for the quadrature with the divergence half-angle equals to 1.27^o.

index i	**Angle,** θ_i $(^o)$	μ_i	**Weight** w_i	**index** i	**Angle,** θ_i $(^o)$	μ_i	**Weight** w_i
1	0.0	1.000000	2.46×10^{-4}	13	98.43	-0.146618	0.29103
2	1.85	0.999479	7.05×10^{-4}	14	115.27	-0.426806	0.265178
3	3.32	0.998322	1.60×10^{-3}	15	132.00	-0.669092	0.21576
4	4.92	0.996315	2.39×10^{-3}	16	148.42	-0.851919	0.14718
5	6.80	0.992976	3.04×10^{-3}	17	163.56	-0.959112	6.57×10^{-2}
6	7.99	0.990304	3.49×10^{-3}	18	170.64	-0.986680	3.72×10^{-3}
7	9.36	0.986680	3.72×10^{-3}	19	172.02	-0.990304	3.49×10^{-3}
8	16.44	0.959112	6.57×10^{-2}	20	173.51	-0.993586	3.04×10^{-3}
9	31.58	0.851919	0.14718	21	175.08	-0.996315	2.39×10^{-3}
10	48.00	0.669092	0.21576	22	176.68	-0.998322	1.60×10^{-3}
11	64.74	0.426806	0.26518	23	178.15	-0.999479	7.05×10^{-4}
12	81.57	0.146618	0.29103	24	180.00	-1.000000	2.46×10^{-4}